




Effects of phosphorus and germanium on oxidation microstructure of Sn–0.7Cu lead-free solders

Chen Liu¹, Jubo Peng¹, Juntao Hu¹, Shanshan Cai^{1,*} , and Xiaojing Wang^{2,*}

¹Yunnan Tin Group (Holding) Co. Ltd, Kunming 650000, China

²Jiangsu University of Science and Technology, Zhenjiang 212003, China

Received: 9 July 2022

Accepted: 3 November 2022

Published online:
7 January 2023

© The Author(s), under exclusive licence to Springer Science+Business Media, LLC, part of Springer Nature 2023

ABSTRACT

In this paper, the oxidation resistance of SCN (Sn–0.7Cu–0.05Ni), SCP (Sn–0.7Cu doped by 0.02 wt% P), and SCNPG solder alloys (Sn–0.7Cu with 0.007 wt% Ge and 0.005 wt% P addition) were investigated at 260 °C in air. Their oxidized surfaces were systematically studied by XPS and SEM-EDS analysis. The results show that SCNPG alloys have better oxidation resistance compared to SCP alloys with more antioxidant additions before oxidation. This may be due to the combined weight of P and Ge in SCNPG alloy surface is higher than that of P alone in SCP alloy after oxidation. Furthermore, for the oxidized surface, P₂O₅ and GeO₂ formed in the outer layer and CuP₂ and FeP exist in subsurface layer. Formation of these oxides and P compounds can be attributed to that Gibbs free energy of oxides is lower than that of P compounds, meaning that oxides are easier to form than P compounds. After the formation of P₂O₅, the excess P forms compounds with negative enthalpy change.

1 Introduction

Sn–0.7Cu solder is one of the high-performing, widely used, low-cost Pb-free solder available in industry. It has been commonly used in wave soldering, solder dipping, and hot air solder levelling applications as a replacement for Sn–37Pb alloy [1–3]. However, the heat input compared to Sn–Pb eutectic has been a great concern, due to the melting point (227 °C) of Sn–0.7Cu is 44 °C higher than that of traditional Sn–Pb eutectic alloy (183 °C). And the maximum heating temperature of the equipment, liquid solder metal during fabrication has also been

correspondingly increased by at least 44 °C. Such a temperature increase will cause the liquid solder oxidation problem and dross generation in a very high volume, which further result in solderability deterioration [4]. According to the research of Shohji et al. and Yen et al., adding a trace amount of alloying elements like Ni and Ge, can greatly improve the oxidation resistance and reliability performance in service [5, 6]. Even 0.05 wt% Ni doped to Sn–0.7Cu solder can significantly reduce the bridging tendency, refine the microstructure, and decrease the thickness of interfacial compounds between solder and under bump metal [7]. The microalloying elements Ge and

Address correspondence to E-mail: sscail0s@alum.imr.ac.cn; wxj@just.edu.cn

Table 1 Chemical compositions of samples measured by optical emission spectrometry

Samples	Nominal compositions (wt%)				Measured compositions (wt%)			
	Cu	Ni	P	Ge	Cu	Ni	P	Ge
SCN	0.700	0.050	–	–	0.065	0.050	–	–
SCP	0.700	–	0.020	–	0.707	–	0.018	–
SCNPG	0.700	0.050	0.005	0.007	0.682	0.032	0.005	0.007

P, differently, are usually enriched on the surface of liquid solder, which affect the liquid oxidation performance depend on the amount of additive. Previous research indicated that minimum content of Ge should reach 0.005 wt% to show an obvious anti-oxidation effect at 280 °C [8]; for P element, 0.007 wt% doping can significantly reduce surface oxidation rate of molten tin in air, while antioxidation ability of molten tin was deteriorated instead of improved when P added was 0.07 wt% [4, 9].

Many experimental studies have been carried out to investigate the oxidation resistance of Sn-Cu solders with P and Ge elements via comparing the surface microstructures before and after oxidation. The microstructure characterization was usually analyzed by X-ray photoelectron spectroscopy (XPS) [4, 9, 10]. However, XPS analysis failed to provide any information on P compounds deteriorating solder fluidity and reliability [11, 12], which were observed by Scanning Electronic Microscopy-Energy Dispersive Spectrometer (SEM-EDS) in a few studies. In addition, previous studies based on XPS analysis present that solder oxidation performance is mainly related to enthalpy change or Gibbs free energy of antioxidant elements and oxygen elements. However, thermodynamic analysis of P compounds and Ge compounds is quite insufficient so far. Therefore, it is necessary to combine SEM-EDS and XPS to obtain comprehensive microstructure information and related thermodynamic analysis to control these compounds.

In this work, Sn–0.7Cu–0.05Ni, Sn–0.7Cu–0.02P, and Sn–0.7Cu–0.05Ni–0.005P–0.007Ge alloys were selected based on the previous investigations. The microstructures of solder surfaces after oxidation with various P and Ge antioxidant additions were systematically characterized by combining with XPS and SEM-EDS analysis. Then, the formation of different phases in oxidized surface was analyzed by thermodynamic analysis. The present systematic microstructure characterization of oxides, compounds of antioxidant additions and related energy

changes can definitively guide solders oxidation performance improvement.

2 Materials and methods

Sn-Cu based solder alloys were prepared by putting pure Sn (99.99 wt%), Cu (99.99 wt%), Ge (99.99 wt%) metals, Sn–0.5Ni, and Sn–5P intermediate alloys in a quartz tube of 15 mm in diameter, melting at 800 ± 3 °C for 3 h. During melting, melts were stirred at least three times before cooling. The nominal compositions of three solder alloys are Sn–0.7Cu–0.05Ni (SCN), Sn–0.7Cu–0.02P (SCP), Sn–0.7Cu–0.05Ni–0.005P–0.007Ge (SCNPG), and their actual compositions were tested by using optical emission spectroscopy (OES) as shown in Table 1.

A 50 g sample was put in an open graphite crucible for melting in air at 260 ± 3 °C. To provide an initial clean liquid metal surface, the original dross was removed from surface using a slag removal tool. Subsequently, the molten alloy was oxidized in air for 2 h at least. Oxide surfaces of liquid metals and appearance solidified alloys were carefully recorded by an iPhone camera after air cooling down. In order to compare the element distribution in different location of alloys, oxidized surface and middle part of the sample were taken for observation.

Surface morphology observations combined with the individual elemental distribution of oxidized alloys surface and dross were performed by Hitachi SU8010 scanning electron microscope equipped with an energy-dispersive spectrometer (EDS). At least 2 EDS mapping images were randomly selected for each sample, and the size of the measured area was $19,822.75 \mu\text{m}^2$. Phase fractions were calculated using ImageJ. Depth profiling of oxidized alloys surface was carried out on a K-alpha X-ray photoelectron spectrometer (XPS) with Al sources. The etching speed is 0.15 nm/s (refer to Si/SiO₂) and mode is low current. To better understand information of

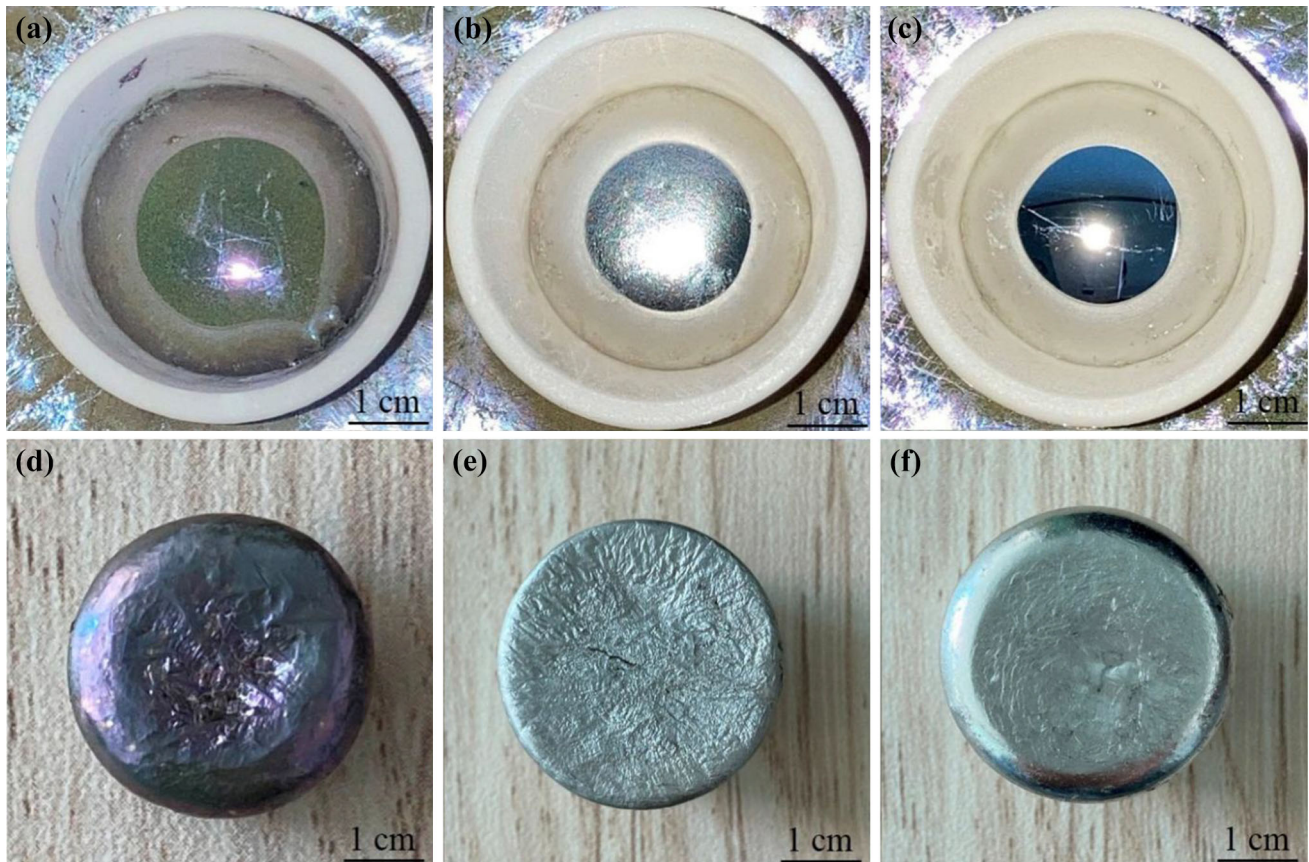


Fig. 1 Oxidation appearances of **a** SCN, **b** SCP, **c** SCNPG after exposure in air at 260 ± 3 °C for 2 h; oxidation appearances of **c** SCN, **d** SCP, **e** SCNPG after air cooling to room temperature

compounds, each alloy with four different regions was conducted by XPS.

3 Results and discussion

3.1 Surface appearance of solder alloys

Figure 1 shows oxidized surfaces of SCN, SCP, and SCNPG at 260 ± 3 °C for 2 h, respectively, and their corresponding oxidized surfaces of air-cooled solidified samples. The surfaces of SCN and SCP liquid solder alloys appear an inhomogeneous purple and gray-white (Fig. 1a, b), respectively. In contrast, the SCNPG liquid alloy surface shows no obvious oxidation color and remains bright (Fig. 1c). Compared with these liquid alloy surfaces, the color of SCN and SCP solidified surfaces deepened (Fig. 1d, e) while SCNPG solid alloy surface keep a metallic sheen (Fig. 1f). Therefore, anti-oxidation effect of SCNPG solder alloy with 0.005 wt% P and 0.007 wt% Ge additions is better than that of SCP solder alloy with

0.02 wt% P alone and SCN solder alloy without antioxidant elements.

3.2 Microstructure characterization and elemental mapping analysis

For above three solder alloys, SEM-EDS was used to conduct comparative analysis on the surface before and after air oxidation, and the dross removed from the molten solder surface. Before oxidation, the distribution of elements from surface of solder alloys is shown in Fig. 2. For SCN and SCNPG solder alloys, needle-like-shaped Cu-Ni-rich phase and Cu-rich phase distributed randomly. These phases are $(\text{Cu}, \text{Ni})_6\text{Sn}_5$, and the rest of Cu-rich phases are Cu_6Sn_5 with a few microns to 50 μm in length and several microns wide [13]. For SCP solder alloy, except Cu_6Sn_5 with an area fraction of $2.76 \pm 0.22\%$, Sn-P compounds with area fraction of $8.38 \pm 5.92\%$ was observed. EDS elemental analysis indicates atomic

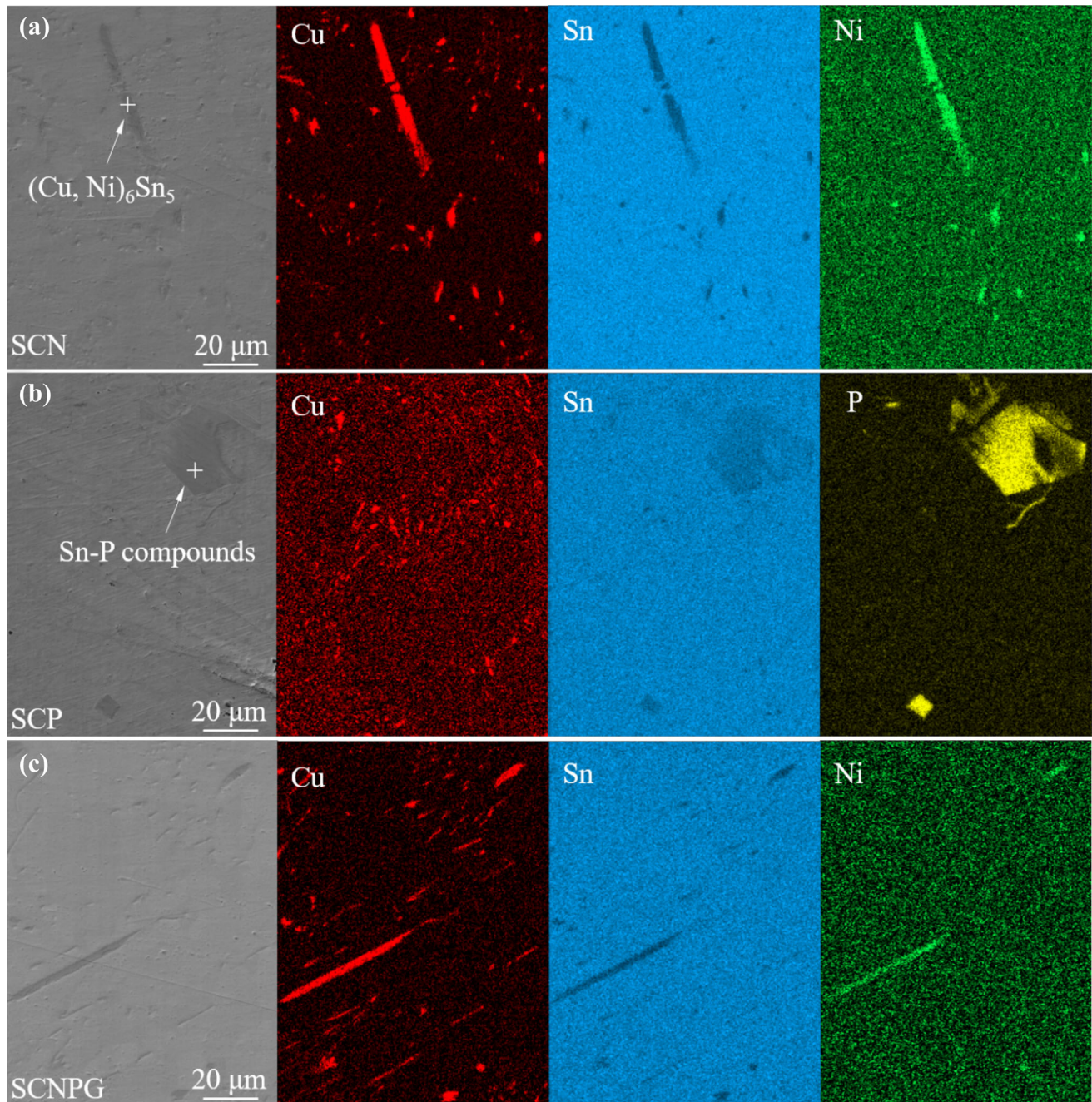


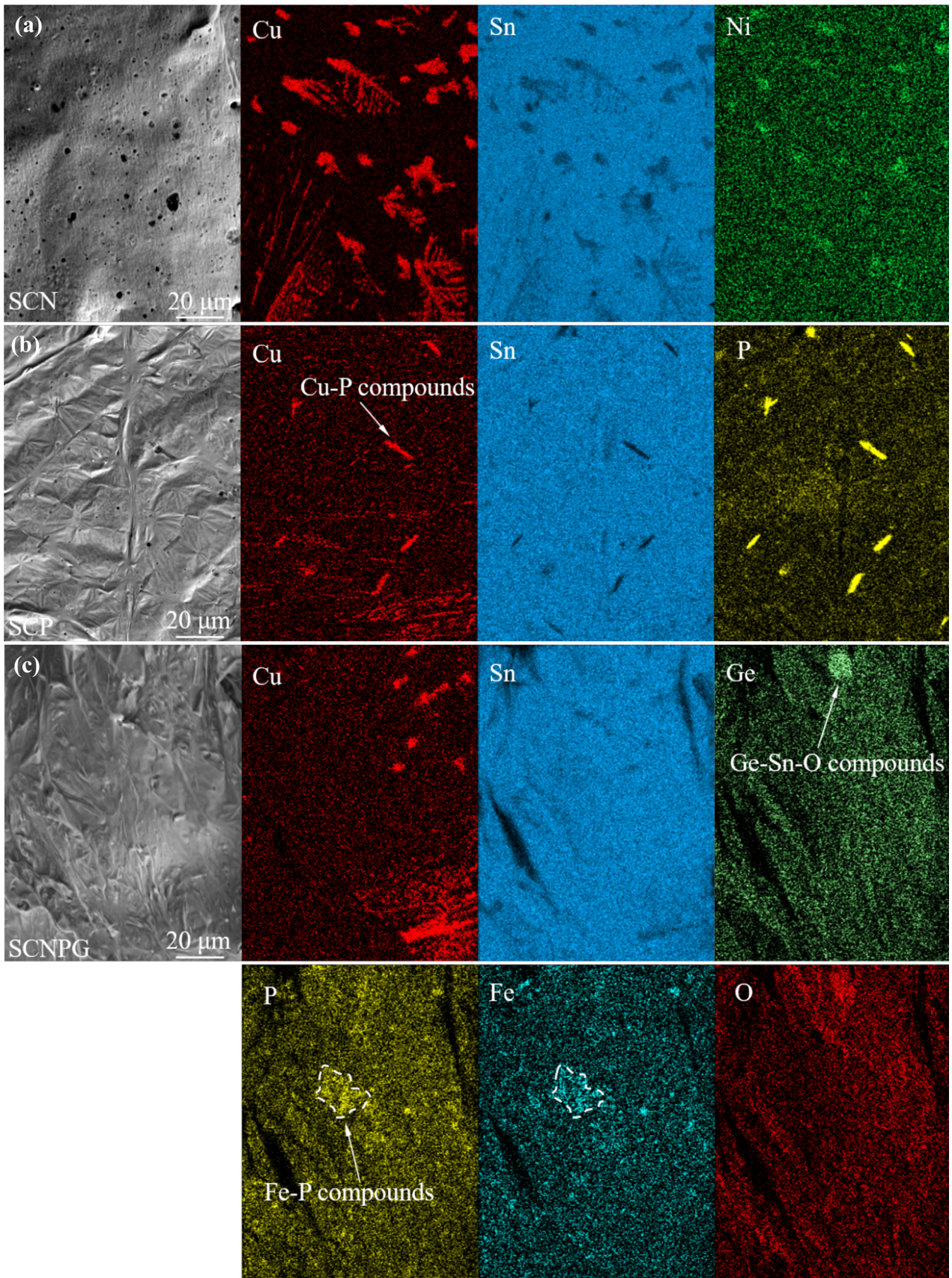
Fig. 2 SEM micrograph and associated EDS elemental mapping of Sn, Cu, Ni, and P of **a** SCN, **b** SCP, **c** SCNPG before oxidation. Note Ge could not be detected

composition of Sn:P in the ratio 56.168:43.832 at% which is likely Sn_4P_3 [14].

After air oxidation, the distribution of elements from oxidized surface of solder alloys is shown in Fig. 3. For SCN alloys, the length of needle-like $(\text{Cu}, \text{Ni})_6\text{Sn}_5$ and Cu_6Sn_5 is up to 20 μm (Fig. 3a), and their area fraction increased to $17.65 \pm 2.23\%$ compared to SCN solder alloys before oxidation with area fraction

Fig. 3 SEM micrograph and associated EDS elemental mapping from oxidation surface of **a** SCN, **b** SCP, **c** SCNPG after air cooling to room temperature

of $6.00 \pm 1.06\%$. For the oxidized surface of SCP solder alloys, needle-like Cu–P phases with an area fraction of $1.66 \pm 0.01\%$ were observed, and the size



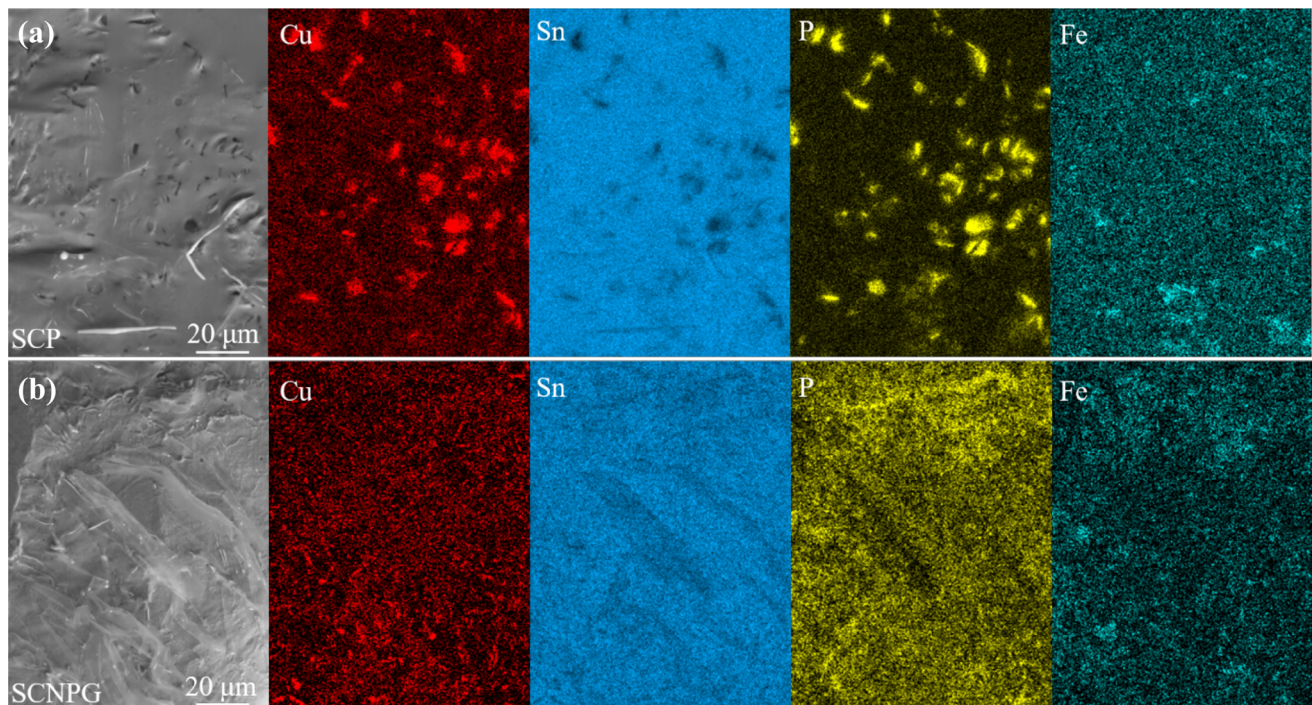


Fig. 4 SEM and EDS elemental mapping for dross of **a** SCP, **b** SCNPG

in length direction reached 10 μm . EDS elemental analysis indicates atomic composition of Cu:P in the ratio 0.5:1 at%. Combined with Cu–P diagram [15], the needle-like Cu–P phases is likely CuP_2 . For the oxidized surface of SCNPG solder alloys, larger Ge–Sn–O compounds were also observed (Fig. 3c) with their atomic compositions of Ge:Sn:O in the ratio of 27.396:17.112:55.492 at% which needs further study. Irregular-shaped Fe–P compounds can also be found in the same sample (shown by arrows in Fig. 3c). EDS elemental analysis indicates that atomic composition of Fe:P is close to 1:1 which may have a composition of FeP [16]. Particularly, atomic emission spectrometer analysis shows the Fe content of SCP and SCNPG solder alloys is about 0.001 wt% and 0.002 wt%, and Cu content is roughly 0.71 wt% and 0.68 wt%, respectively. Namely, Fe element content and Cu element content in two alloys differ by 3 orders of magnitude, but Fe element is much easier to form FeP intermetallic compounds. This result is consistent with previous research reporting that the content of Fe element in SAC305-0.3Ti alloy is only 0.005 wt%, but trace Fe element will be enriched on the surface and then form (Ti, Cu, Fe) Sn_2 [17].

The element distribution in the dross of two solder alloys containing P are displayed in Fig. 4. The area fraction of CuP_2 and FeP is $6.22 \pm 1.54\%$ and

$3.92 \pm 0.18\%$ in SCP dross, respectively. In contrast, they are only $2.78 \pm 0.18\%$ and $3.10 \pm 0.17\%$ in SCNPG dross, respectively. Obviously, the amount of CuP_2 and FeP in SCP solder alloy dross is significantly higher than that of SCNPG solder alloy.

As mentioned above, intermetallic compounds changed before and after air oxidation. Table 2 summarizes the types of these compounds from surface of unoxidized samples, surface and dross of oxidized samples as well as middle part of oxidized samples. Before oxidation, P compounds were not observed on surfaces of SCNPG alloy with 0.005 wt% P while Sn_4P_3 phase appears on the surface of SCP alloy containing 0.02 wt% P. This suggested that 0.02 wt% P already exceeded the saturated solid solution degree of P element in the base alloy, results in that the remaining parts of P element precipitate to form Sn_4P_3 . For SCP and SCNPG alloys after oxidation, a large amount of CuP_2 and FeP compounds distribute on oxidized surface and dross. However, it is difficult to observe any form of P compounds inside of middle part of oxidized samples, indicating that P easily enriched on liquid solder surface. Moreover, because the surface activity of oxygen element is higher than that of phosphorus element, the original surface equilibrium system of solder alloys is broken after oxidation [18]. This may explain that Sn_4P_3

Table 2 Types of intermetallic compounds present in three alloys

Alloys	Surface of unoxidized samples	Surface and dross of oxidized samples	Middle part of samples
SCN	Cu ₆ Sn ₅ (Cu, Ni) ₆ Sn ₅	Cu ₆ Sn ₅ (Cu, Ni) ₆ Sn ₅	Cu ₆ Sn ₅ (Cu, Ni) ₆ Sn ₅
SCP	Sn ₄ P ₃ Cu ₆ Sn ₅	CuP ₂ , FeP Cu ₆ Sn ₅	Cu ₆ Sn ₅
SCNPG	Cu ₆ Sn ₅ (Cu, Ni) ₆ Sn ₅	CuP ₂ , FeP Ge–Sn–O compound	Cu ₆ Sn ₅ (Cu, Ni) ₆ Sn ₅

compound disappears after oxidation. For 0.007 wt% Ge addition, Ge is also hard to trace except for oxidized surface due to elemental enrichment [4].

3.3 Depth profiling of oxidation surface

Figure 5a–c shows the XPS depth profiles of solidified surface of SCN, SCP, and SCNPG alloys after oxidation by Ar ion etching. Figure 5c highlights the existence of Sn, Cu, O, P, and Ge in the surface, which is in accordance with EDS results as shown above. The Sn3d_{5/2} and Sn3d_{3/2} (hereinafter referred to as 3d5 and 3d3) peaks correspond to 485.1 eV and 493.5 eV, respectively. With the progress of sputtering, oxidation state peaks of Sn3d spectra gradually decreased, while Sn metal peaks gradually increased (Fig. 5a). After 120 s sputtering with 18 nm from surface (Fig. 5c), two sub-peaks of Sn3d in SCNPG solder with 0.005 wt% P and 0.007 wt% Ge have both single-peak structures, while two sub-peaks of Sn3d in SCN alloys and SCP alloys are bimodal structures, implying that Sn metal and Sn oxidation state coexist. These tin oxides could be SnO, SnO₂, or their mixture, confirmed by many previous studies [19].

Additionally, peak intensities of O1s spectra of three alloys gradually weakened with sputtering, but their decreasing rates differ (Fig. 5b). Table 3 summarized statistical data of O content in three alloys oxide layer within 300 s after XPS sputtering. For SCN, SCP, and SCNPG alloys, their initial oxygen contents are 24.99 ± 0.33 wt%, 24.92 ± 1.35 wt%, and 24.26 ± 1.46 wt%, respectively. This means that their initial O content is rough equal. To better represent the reduction of O content after different sputtering time, we normalize these values using the initial value of 24.72 wt%. That is, their values are divide by 24.72 wt%. After 60 s sputtering (Fig. 5c), the O content of SCN, SCP, and SCNPG alloys decline significantly to 54%, 46%, and 29%. Then, the O

content of SCN and SCP alloys decrease by about 14%, while the O content of SCNPG alloy by about 21% at 120 s. After 300 s sputtering, the O content of SCNPG alloy tends to saturate with 8%, which is about 1/3 of SCN alloys and 1/2 of SCP alloys, respectively. Obviously, 0.007 wt% Ge and 0.005 wt% P addition could effectively reduce O content and consequently reduce the thickness of oxide film.

Variation of surface P and Ge with etching time displays a slight decrease at first and then tends to be flat (Fig. 5c). Figure 6 illustrates the binding energy of P and Ge solutes in surface oxide layer of SCP alloy and SCNPG alloy. The binding energies of P2p are 133 eV and 128.5 eV, corresponding to P⁵⁺ and P³⁻, respectively. The binding energy of 133 eV peak might be P₂O₅ or metal phosphate, which supported by previous reports [4, 9]. Besides, P₂O₅ has strong hydrophilicity which readily reacts with water to generate phosphoric acid. Thus, it is likely that phosphate in this paper originated from the transformation of P₂O₅. Moreover, when sputtered to 36 nm from oxidized surface, the peak representing metal phosphide appeared, with the peak intensity gradually increasing in depth direction as shown in Fig. 6a. Combining with SEM-EDS results, these phosphide may be CuP₂ and FeP.

For SCNPG alloy with less P, a decrease of P content leads to low intensity of phosphate peak and only one layer of phosphide peak exists (Fig. 6b). Transition from phosphate to phosphide with etching time has also been observed in previous studies [9]. Therefore, for P containing solder alloys after oxidation, P element mainly exists in the form of P₂O₅ in outermost layer, and mainly exists in the form of CuP₂ and FeP in subsurface layer.

Figure 6c illustrates high-resolution Ge 2p3 spectra changing with etching time. Combing with previous research [10], Ge element in oxide layer of SCNPG

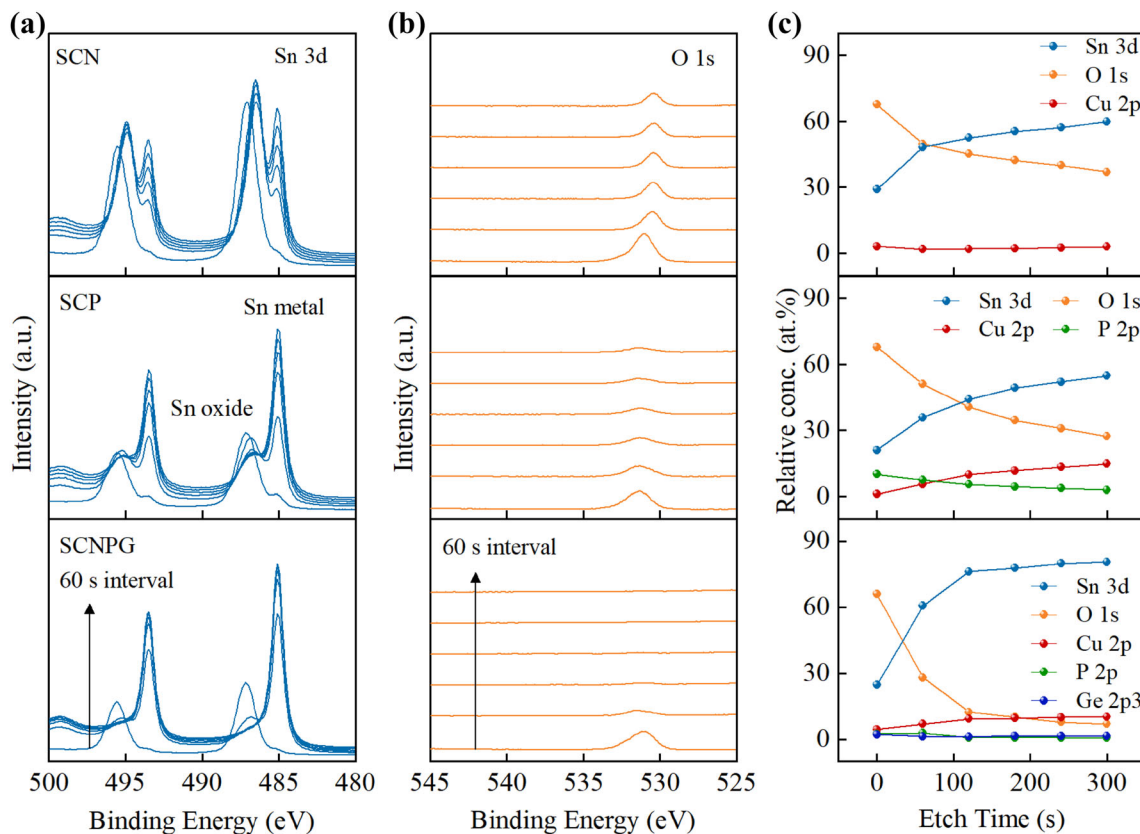


Fig. 5 Depth profiles of **a** Sn 3d and **b** O 1s, and **c** relative concentrations, excluding Nickel and trace impurities, in 0.15 nm/s increments from oxidation surface to 45 nm. The top is depth

profile and relative concentrations of SCN, with the middle and bottom are depth profile and relative concentrations of SCP and SCNPG, respectively

Table 3 Statistical data of O, P, and Ge contents in three alloys oxide layer within 300 s after XPS sputtering

Etch time (s)	SCN-O (wt%)	SCP-O (wt%)	SCP-P (wt%)	SCNPG-O (wt%)	SCNPG-P (wt%)	SCNPG-Ge (wt%)	SCNPG-(Ge + P) (wt%)
0	24.99 ± 0.33	24.92 ± 1.35	4.04 ± 1.17	24.26 ± 1.46	2.78 ± 0.71	2.28 ± 0.56	5.06 ± 0.90
60	13.42 ± 0.49	11.47 ± 1.43	3.42 ± 0.64	6.97 ± 2.18	3.16 ± 0.90	1.09 ± 0.36	4.25 ± 0.97
120	10.27 ± 0.49	7.77 ± 1.95	1.17 ± 0.43	1.89 ± 0.14	0.54 ± 0.21	0.65 ± 0.19	1.19 ± 0.28
300	5.96 ± 1.09	3.70 ± 1.25	0.78 ± 0.31	1.80 ± 0.51	0.43 ± 0.26	0.63 ± 0.11	1.06 ± 0.28

alloy is in the form of GeO_2 . Even adding dozens of ppm levels of Ge and P, their segregation on the oxidized surface were wildly observed. Part of Sn^{2+} in the SnO lattice which belongs to *n*-type semiconductor is replaced by Ge^{4+} after adding traces Ge, resulting in a decrease in oxidation rate and improvement the oxidation resistance of solder alloys [8, 20]. The existence of P^{5+} may indicate that anti-oxidation mechanism of P element and Ge element is similar.

Table 3 also shows the statistical data of P and Ge contents within 300 s after XPS sputtering. Compared

with the small error bar of the O content, both error bars of P and Ge contents are larger due to inhomogeneous distribution of P and Ge with minor addition. After sputtering from 0 to 300 s, the contents of P element in SCP are higher than those in SCNPG samples, which is in agreement with SEM results shown in Figs. 3 and 4. For both P containing alloys, P contents kept unchanged at 60 s and then decreased to about 20% of their initial values at 120 s which is equal to the value at 300 s. In contrast, Ge content of SCNPG alloys decline to 48% of its initial values at 60 s and then drop to about 29% of their

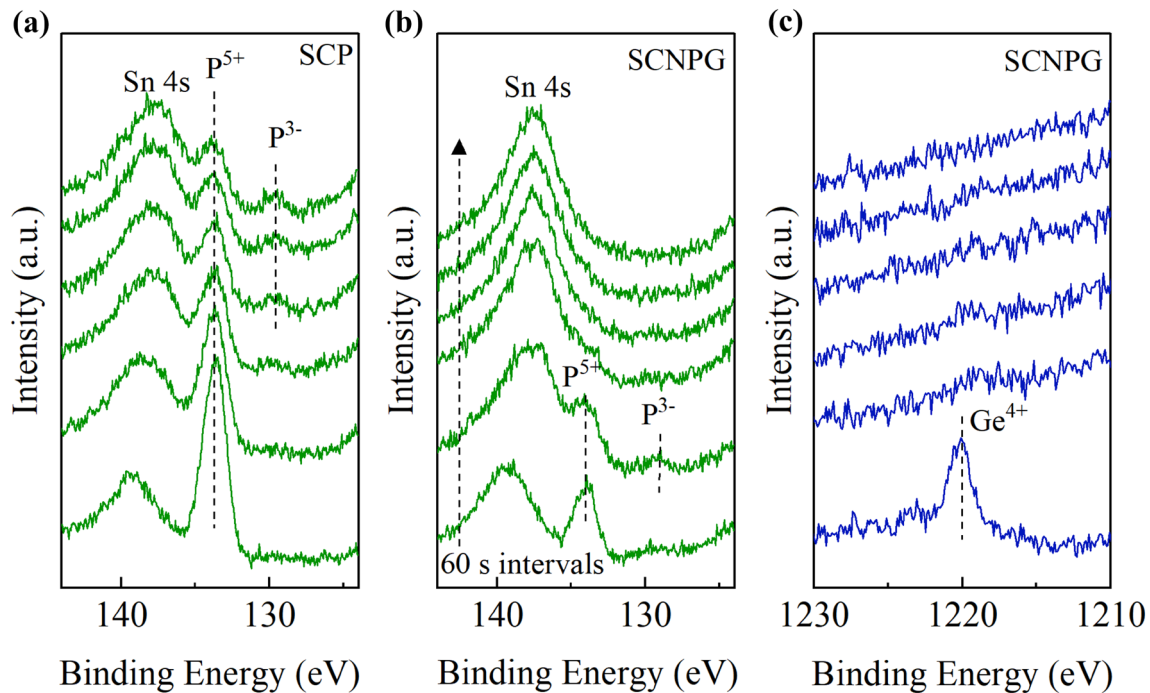


Fig. 6 Depth profiles of **a** P^{5+} and P^{3-} of SCP, **b** P^{5+} and P^{3-} of SCNPG, and **c** Ge^{4+} of SCNPG. Each spectrum can be distinguished by its spectral features

initial values at 120 s which is also equal to the value at 300 s. As discussed above, O content variation for these alloys shows a large drop at 60 s etching time, and the O content of P containing alloys exhibit a large difference at 60 and 120 s. Thus, by comparing the content of P and Ge elements corresponding to sputtering time, it is found that the combined weight of P and Ge in SCNPG alloy is higher than that of single P in SCP alloys. Accordingly, this may cause SCNPG samples with better antioxidant performance even though it contains fewer antioxidant ingredients compared to SCP samples before oxidation.

3.4 Thermodynamic analysis of oxides and intermetallic compounds

Based on the results of SEM-EDS, P needs to exceed a certain content to form compounds with Sn, leading to the formation of Sn_4P_3 before oxidation in SCP solder, and then disappear after oxidation. Simultaneously, CuP_2 and FeP form after oxidation. The corresponding XPS has verified that P element mainly exists in the form of P_2O_5 in outermost layer, and mainly exists in the form of CuP_2 and FeP in subsurface layer. In contrast to Ge, it tends to form GeO_2 . In order to understand these results, Gibbs free

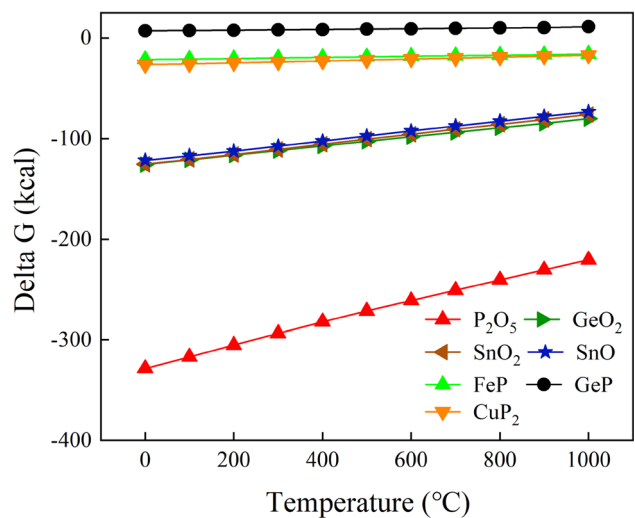


Fig. 7 Standard Gibbs free energy diagram of oxide and part of intermetallic compound mentioned above

energy of oxides and P compounds in the range of 0 to 1000 °C is calculated using HSC Chemistry 6.0 software (Fig. 7). Accordingly, Gibbs free energy of oxides is lower than that of P compounds implying that oxides are easier to form than P compounds.

For oxides, the order of Gibbs free energy is $P_2O_5 < GeO_2 \approx SnO_2 \approx SnO$. Similarly, the order of oxide enthalpy of formation at 600 K is

$P_2O_5 < GeO_2 \approx SnO_2 < SnO$ [21]. Experimental results have also verified elements P and Ge are easier to form P_2O_5 and GeO_2 , respectively. Thus, P_2O_5 is easily formed on surface, followed by GeO_2 , SnO_2 , and SnO .

Because HSC chemistry 6.0 lacks Gibbs free energy of Sn_4P_3 , thermodynamic enthalpy of P compounds is used. Enthalpy change required for P element and Sn, Cu, Fe to form compounds is -7.5 kJ mol^{-1} , $-17.5 \text{ kJ mol}^{-1}$, and $-39.5 \text{ kJ mol}^{-1}$, respectively [21]. These are all lower than enthalpy changes of Sn–Cu with 7 kJ mol^{-1} , Sn–Fe with 11 kJ mol^{-1} , and Cu–Fe with 13 kJ mol^{-1} . Therefore, P easily forms intermetallic compounds with Fe, Cu, and Sn, and preferentially forms FeP compounds. Furthermore, comparing with Gibbs free energy of GeO_2 , Gibbs free energy of Ge–P compound becomes greater than zero (Fig. 7). This can explain that Ge–P compound could not be found in experiment, even though Ge element tends to concentrate on oxidized surface.

Observation of FeP compounds is worth noting due to the enrichment of trace Fe elements on the surface. From Fe–Cu–P ternary phase diagram [22], Fe–P compounds are preferentially generated. Only when phosphorus content and copper content exceed 8 wt% and 80 wt% at the same time, Cu–P compound might be found. P element in Sn–0.7Cu–0.05Ni–0.01Ge–0.01P solder alloy accelerates erosion of an iron plated soldering tool tip and stainless steel wave solder machine parts in factory production [7]. These phenomena can be mainly attributed to that FeP compounds easily form even with trace Fe content.

Additionally, P element in solder alloy also deteriorates other properties due to easy formation of compounds. First, adding P element to Ni containing solder will increase the amount of solder oxide surface slag. Adding 0.001–0.003 wt% P element, Ni–Sn–P intermetallic compounds generated on oxidized surface, resulting in a significant increase in the amount of slag. Secondly, P element also affects fluidity of solders. Ni–xP compounds in Sn–0.7Cu–0.05Ni–0.07P alloy reduce fluidity of solders [7]. Thus, this paper can provide a theoretical basis for improvement of property degradation caused by P elements addition.

4 Conclusion

Sn–0.7Cu solder alloy with 0.007 wt% Ge and 0.005 wt% P addition has better oxidation resistance than Sn–0.7Cu solder alloy with 0.02 wt% P addition at

260 °C in air, which can be attributed to the combined weight of P and Ge elements in SCNPG alloy being higher than that of single P element in SCP alloy. P element exists in the form of P_2O_5 in outer surface layer of the oxidized surface, while in the subsurface layer it mainly exists in the form of CuP_2 and FeP . Gibbs free energy of oxides is lower than that of P compounds; thus, oxides are easier to form than P compounds. The content of Fe element is at least 3 orders of magnitude lower than that of Cu element in solders containing P, but P element preferentially forms FeP compounds with Fe element. Ge element mainly exists in the form of GeO_2 on oxidized surface of solders. P element easily forms intermetallic compounds with Sn, Cu, and Fe. It is still difficult to form compounds with Ge, because Gibbs free energy of Ge–P compound becomes higher than zero.

Acknowledgements

This research was supported by the Yunnan Science and Technology Major Project (Grant number 202002AB080001) and the Research and Development Funding of Yunnan Tin Group (Holding) Co, Ltd. The authors would like to thank Shiyu Yang in Yunnan Tin Group (Holding) Co. Ltd for conducting SEM/EDS experiments.

Author contributions

CL: experimental design, carrying out measurements, writing—original draft. JP: funding acquisition, writing—review and editing. SC: writing—review and editing. XW: conception, writing—review and editing. JH: carrying out measurements of XPS and analysis.

Funding

This study was funded by Yunnan Science and Technology Major Project (Grant number 202002AB080001).

Data availability

The data used to support the findings of this study are available from the corresponding author upon request.

Declarations

Conflict of interest The authors declare no conflict of interest.

References

1. L. Yang, *J. Mater. Sci. Mater. Electron.* **24**, 1405 (2013)
2. G. Zeng, S. Xue, L. Zhang, L. Gao, Z. Lai, J. Luo, *J. Mater. Sci. Mater. Electron.* **22**, 1101 (2011)
3. X. Wu, J. Wu, X. Wang, J. Yang, M. Xia, B. Liu, *J. Mater. Sci.* **55**, 3092 (2020)
4. A.P. Xian, G.L. Gong, *J. Electron. Mater.* **36**, 1669 (2007)
5. I. Shohji, S. Tsunoda, H. Watanabe, T. Asai, M. Nagano, *Mater. Trans.* **46**, 2737 (2005)
6. Y.W. Yen, Y.C. Chiang, C.C. Jao, D.W. Liaw, S.C. Lo, C. Lee, *J. Alloys Compd.* **509**, 4595 (2011)
7. K. Nogita, C.M. Gourlay, J. Read, T. Nishimura, S. Suenaga, A.K. Dahle, *Mater. Trans.* **49**, 443 (2008)
8. Q.M. Wang, G.S. Gan, Y. Du, D. Yang, G. Meng, H. Wang, Y.P. Wu, *Mater. Trans.* **57**, 1685 (2016)
9. A.P. Xian, G.L. Gong, *J. Mater. Res.* **23**, 1532 (2008)
10. K.M. Watling, A. Chandler-Temple, K. Nogita, *Mater. Sci. Forum* **857**, 63 (2016)
11. Q.T. Xuan, M.A.A. Mohd Salleh, S.D. McDonald, K. Nogita, *Solid. State Phenom.* **273**, 9 (2018)
12. K. Nogita, M.A.A. Mohd Salleh, X.Q. Tran, J. Read, S. Smith, S.D. McDonald, *Mater. Sci. Forum* **857**, 49 (2016)
13. L. Zhang, Z.Q. Liu, *J. Mater. Sci. Mater. Electron.* **31**, 2466 (2020)
14. R. Ganesan, A. Ciccio, G. Gigli, H. Ipsier, *Int. J. Mater. Res.* **102**, 93 (2011)
15. S.P. Gordienko, G.S. Viksman, *Sov. Powder Metall. Met. Ceram.* **24**, 573 (1985)
16. R. Vogel, G. Zwingmann, *Arch. Für Das Eisenhüttenwes* **26**, 631 (1955)
17. Z.L. Ma, H. Shang, A.A. Daszki, S.A. Belyakov, C.M. Gourlay, *J. Alloys Compd.* **777**, 1357 (2019)
18. X.M. Xue, H.G. Jiang, Z.T. Sui, B.Z. Ding, Z.Q. Hu, *Metall. Mater. Trans. B* **27**, 71 (1996)
19. F.Y. Hung, H.M. Lin, P.S. Chen, T.S. Lui, L.H. Chen, *J. Alloys Compd.* **415**, 85 (2006)
20. F.T. Cao, Z.Q. He, T.G. Wang, Q.X. Fan, Y.M. Liu, J.T. Tao, G.Y. Gao, X.B. Luo, J.B. Peng, S.S. Cai, *Mater. Lett.* **314**, 7 (2022)
21. A. Takeuchi, A. Inoue, *Mater. Trans.* **46**, 2817 (2005)
22. J. Miettinen, G. Vassilev, *J. Phase Equilibria Diffus.* **35**, 469 (2014)

Publisher's Note Springer Nature remains neutral with regard to jurisdictional claims in published maps and institutional affiliations.

Springer Nature or its licensor (e.g. a society or other partner) holds exclusive rights to this article under a publishing agreement with the author(s) or other rightsholder(s); author self-archiving of the accepted manuscript version of this article is solely governed by the terms of such publishing agreement and applicable law.